AutoSoft®

# Contactless Rail Profile Measurement and Rail Fault Diagnosis Approach Using Featured Pixel Counting

## Gulsah Karaduman[*], Mehmet Karakose, Ilhan Aydin, Erhan Akin

Firat University, Computer Engineering Department, 23100, Elazig, Turkey,

**ABSTRACT**
The use of railways has continually increased with high-speed trains. The increased speed and usage wear on the rails poses a serious problem. In recent years, to detect wear and cracks in the rails, image-based detection methods have been developed. In this paper, wears on the surface of railheads are detected by contactless image processing and image analysis techniques. The shadow removal algorithm with a minimal entropy method is implemented onto the noise-free images to eliminate the light variations that can occur on the rail. The Hough transform is applied on the noise and shadow free image in order to determine the rail edge and the KNN nearest neighbour algorithm is applied the image to detect the surface of the railhead at the same time. Both of these methods result in new images that are combined. Therefore, minimum errors are seen in detection of rail wear using this method.

**KEY WORDS**: Rail profile, Hough transform, shadow removal, KNN.

## 1  INTRODUCTION

RAILS are the most important components of railways. Train wheels and rails are in contact during transportation on railways. Due to the friction resulting from the contact, the wear appears on the rail (Karaduman, Karakose, & Akin, 2012). The wear on the rails over time can cause some adverse situations, namely; transportation safety hazards, rail-wheel relationship deterioration of the track, not seeing the formation of an accident, occurrence of serious energy loss and friction-induced vibration and noise increases (Chen, Roberts, & Weston, 2018). If the rails are regularly inspected and maintained, the wear and faults on the rail can be detected without becoming dangerous, and this deterioration can be intervened and corrected early. Traditionally, deterioration on the rail was detected by hand by a trained person. This examination is slow and dangerous. It also depends on the perception of the person. In another conventional method, the rail is inspected by means of special inspection vehicles in contact with the rails. As these vehicles come into contact with the rails, they cause wear at the same time when examining the rails.

Contactless detection of wear on the rails is preferred, because it is not destructive to the rails. There are several studies shown in literature for non-contact detection of rail wear. Alippi et al (2002)

composite rail profile measurements on the railways. A pre-processing algorithm has obtained the area that contains the rail profile in the image that is taken by a laser scanner camera and the rail profile is restricted using the neural network techniques (Alippi, Casagrande, Fumagalli, Scotti, Piuri, & Valsecchi, 2002). Alippi et al. (2000) proposed an embedded system methodology for real time rail profile analysis at railways. Faiz et al. (2009) analyzed the information of the rail profile for all UK railways. Two CCD cameras monitored the rail and the laser source and regions with disrupted rail profiles was determined. Zhiping et al. (2010) also carried out a rail profile irregularity's wavelet transform for a Beijing-Tianjin inter-city high-speed railway. Causes and location of the rail disorders, which are taken from different periodic components, can be determined using a wavelet transform and power spectrum density analysis. The results of the wavelet analysis evaluated the quality of the rail construction at the railways and were able to guide the rail maintenance. Van et al. (2009) proposed a comprehensive approach to the modeling wear and tear on the rail. Additionally, Zumpano et al. (2006) presented a new damage detection technique to determine the structural surface defects on the rails. The results showed that the proposed method can be successfully used to find the location of the damage. Roohi et al. (2016) proposed a

CONTACT Gulsah Karaduman ✉ gkaraduman@firat.edu.tr

deep convolutional neural network that analyzes image data of the rail to detect wear on the rail surface. The results are better than other network architectures. To evaluate the condition of the rail surface, Ma et al. (2016) applied an automatic texture classification method to the rail images. They obtained 82% accuracy in their experiments. Hu et al. (2010) proposed a method based on morphology with a multi-scale and dual-element to detect heavy rail surface deterioration. They have reduced the detection rate compared to conventional methods.

In this paper, wear and cracks on the surface of the rail head are determined. The images that are captured by the camera are prepared for image processing and analysis operations. To perform the transactions, the image is converted to a gray level image format. The image is then taken from the railways while the train is moving. Therefore, the image can be distorted. Noise removal filters are then applied to provide a clearer image by removing these disruptions. The applied filters are Gaussian and mean filters. The grey image is adjusted to the shadows to escape the effects of the light variations that can occur on the rail. Shadows may occur due to the effects of light and objects on the rail, resulting in the shadows that cause different shades. These shadows can pose problems for detection based on the color segmentation. To avoid such problems, the shadow removal process is carried out. Separate gradation for each color layer is formed on RGB images and then combined into one image in the grayscale and it is free from the shadow image scanning angle according to the direction of the arrival of light. After this operation, the image is converted to black-and-white by determining a threshold. Then, the obtained image portions are determined by using the nearest neighbor classification. After determining the rails nearest neighbor classification, the rail head is detected with the Hough transform. The parts representing the rail in the image obtained by the nearest neighbor algorithm are selected and the remainder of the image is removed. Both of these methods result in new images, which are combined. There is a minimum error set to detect the rail wear. Finally, the detected rail head surface is shown marked on the video and step-by-step the same procedure is repeated on the next image.

In this paper, two approaches are considered. One is the Rail Measurement Approach and the other is the Fault Diagnosis Approach. In the Rail Measurement Approach, the point cloud of the rail was formed with a laser scanner system. Using this point cloud, the rail profile measurement is performed and the depth information of the surface of the rail is obtained. At the same time the geometry of the rail is obtained. The obtained rail profile measurement, surface depth information and rail geometry are used as a reference in the fault diagnosis approach. Previous studies have been able to detect more defects in the rails under certain conditions. In the Fault Diagnosis Approach,

detection will be performed independently from the ambient light due to removing variations in the light. Additionally, two different methods using the surface of the rail head obtained two different results. These two results display the same image as combined. This reduces the error rate in detecting wear on the rail head surface. In the proposed method, wear on the surface of the rail head can be detected independent of the ambient light and can be detected without contact.

## 2    RAIL MEASUREMENT APPROACH

RAIL control is of great importance for railway maintenance and should be done on a regular basis (Jie, Siwei, Qingyong, Hanqing, & Shengwei, 2009). An expert carries out monitoring and inspection of rails shown in traditional methods. In this method, the expert monitors the rail in a car or on foot along the rail with his eyes. The expert who carries out this method decides whether the rail is defective or not with his own criteria. This method is limited to what the experts can see on the rails, and varies according to expert criteria. Moreover, it requires human resources and is slow. Even today, another traditional method used measures the rail profile by measuring instruments called Robel-A, Robel-B or SKM. Lateral and vertical wear in the rails are determined with these tools. This instrument is properly installed on the rail and the ballast under the rail should be cleaned in order to make measurements with the instruments. This method of measurement cannot be performed for each rail in space. In addition, this method requires human resources and is slow (Kaewunruen, & Remenrikov, 2007). Another conventional method shows the rails are controlled by a contact method. Mechanical devices that contact the rail move along the rail. With reference to the figures that occur due to the friction on the rails, graphs of the rail faults are obtained. This method provides accurate results and is fast (Zerbst, Lunden, Edel, & Smith, 2009). However, this method's disadvantage is the damage caused by contact when the rails are checked. Rail contact on mechanical devices causes robust rail grinding or it can increase defective rail failure (Oukhellou, Debiolles, Denoux, & Aknin, 2010). In recent years, due to the disadvantages of conventional methods, control of the railways is performed using image processing and laser technologies. These technologies are not manual, so they are more durable and reliable, and human resources are not required. These technologies are not damaging the rail, because there is no contact on the rail itself. More importantly, high-speed non-contact maintenance can be performed (Van, Maitoumam, Moumni, & Roger, 2009).

In this paper, we created an experimental setup with a laser source and a CCD camera. Laser welding is performed by sending horizontal and vertical laser lines. Using the obtained laser beam images, the point cloud of the rail was formed. Through special software, these point clouds have been used to create

the rail profile, meaning the rail profile measurement was performed without contact. Figure 1 shows the experimental setup of the rail profile measurement.
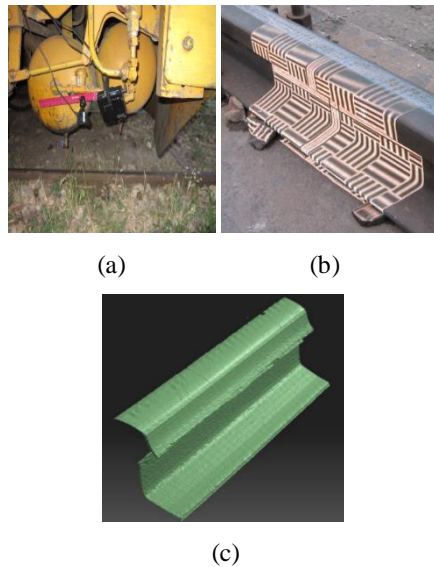


(a)                    (b)

(c)

**Figure 1.  Experimental Setup of the Rail Profile Measurement (a) Laser Source and Camera (b) Scanned Rail (c) Point Cloud of the Scanned Rail.**

## 3    FAULT DIAGNOSIS APPROACH

THE designed system is a study carried out on the detection of wear on the railheads. The flow diagram in Figure 2 shows the analysis of the image from the camera and the determination of the railhead surface. Wear on the surface of the railhead is determined by following these steps, which are in accordance with the algorithm. The proposed method steps are as follows:

In Step 1, the video images captured by the camera (frame) are prepared for image processing and analysis operations. Figure 3 shows the steps of image processing.

In Step 2, first the image is converted to a grayscale level to perform transactions across the image. The image is taken from the railways while the train moves, meaning the image can be distorted. Noise removal filters are applied to provide a clearer working image by removing these disruptions. The applied filters are Gaussian and mean filters.

In Step 3, the gray image is adjusted to the shadows to escape the effects the light variations that can occur on the rail.

**Shadow removal with minimum entropy method:** Shadows may occur with effects of light and objects on the rail. The resulting shadows cause different shades on the rails. These shadows pose problems for detection when using color segmentation. To avoid such problems, the shadow removal process is carried out. A separate gradation for each color layer is formed on the RGB images. The distance between the dots is calculated with the

Euclidean distance calculation formula and classes are created according to the specified range.
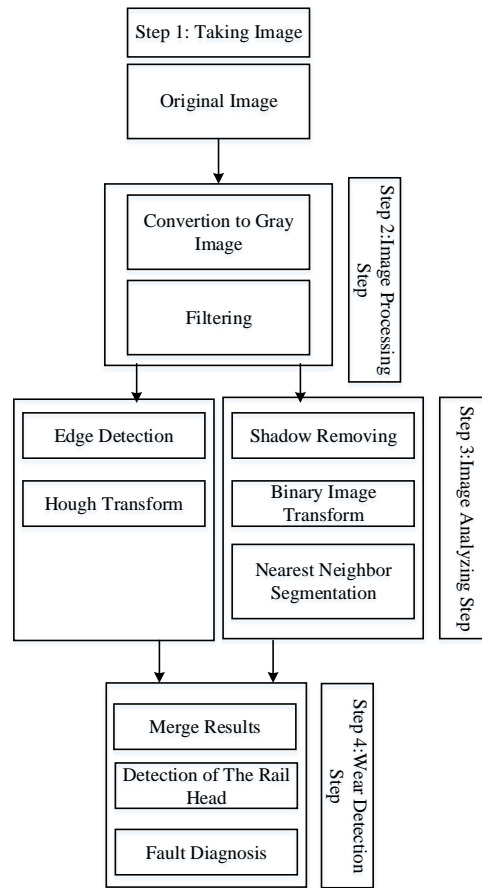


**Figure 2.  Flow Diagram of the Algorithm**
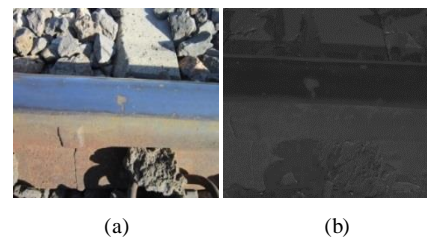


(a)                    (b)

**Figure 3. Image Processing Steps a) Original Image b) Filtered and Converted to a Grayscale Level Image.**

RGB images are pulled from the shadows with a minimum entropy method (Finlayson, Drew, & Lu, 2009). First, the geometric mean is calculated for this process. The calculation of the geometric mean is given in equation (1).

$$G_{mean} = \sqrt[3]{R.G.B} \qquad (1)$$

where R, G, B is the Red, Green, and Blue values for each pixel and  $G_{mean}$  is geometric mean value.

$$C_k = \frac{R_k}{G_{mean}}$$ (2)

where Rk is the Red value for the calculated pixel, $G_{mean}$ is the geometric mean for the calculated pixel, and $C_k$ is color constant, $k$ is the brightness value of the corresponding pixel.

$$P_k = \log(C_k)$$ (3)

where $P_k$ is the section that is falling plane, $C_k$ is color constant, $k$ is the brightness value of the corresponding pixel. Figure 4 shows vertical each $P$ plane due to by geometric mean result.
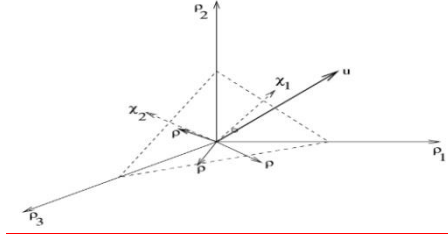


**Figure 4.** Vertical each p Plane Representation due to the Geometric Mean Result (Roohi, Hajizadeh, Nuriez, Babuska, & Schutter, 2016).

$$x = U_p, x \text{ is } 2x1$$ (4)

where U is a 2×3 vertical matrix, $P$ is the section that is falling plane and U returns three vectors of $P$ to the coordinate system.

In the final step of the shadow detection stage, the right projection angle is found and is written in equation (5), and the gray image is obtained.

$$I = x_1 \cos\theta + x_2 \sin\theta$$ (5)

where I is pixel matrix of the gray image.

As a result, the straightened direction that is obtained by minimum entropy is suitable for removing shadows. Entropy is calculated by equation (6).
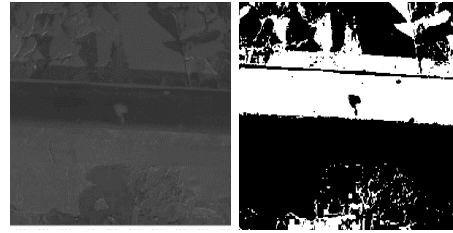
$$\eta = -\sum i p_i(I) \log(p_i(I))$$ (6)

**Nearest neighbor classification:** The image is converted to a black-and-white image with the determination of a threshold after this operation. After this image, portions that are obtained by using the nearest neighbor classification are determined. The important thing is that the properties of each class are defined clearly in advance. The number of the nearest neighbors and the threshold and similarity measurement criteria affect the performance of the method.
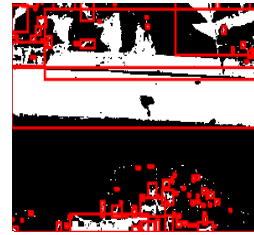
Hough transform: After determining the rail with the nearest neighbor classification, Hough transform is used to determine the rail head. Lines on the image are determined by the Hough transformation. Wear and errors occur in the rail surface in the same direction

are determined quickly and efficiently by the Hough transform that improved in order to make the determination line and circle-like shapes in an image. Figure 5 shows the image analysis steps.

In Step 4, the parts representing the rail in the image obtained by the nearest neighbor algorithm are selected and the remaining parts are removed. Both of these methods result in new images that are combined. A minimum error is determined for the detection of rail wear. Finally, the detected rail head surface is shown marked on the video and step-by-step the same procedure is repeated on the next image. Figure 6 shows combining the images.
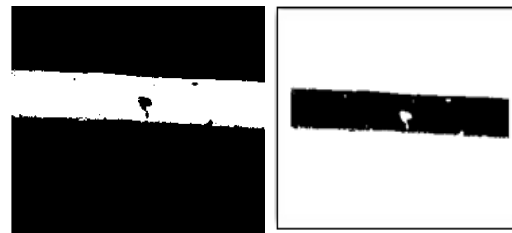


(a)                    (b)



(c)

**Figure 5.** Image Analysis Steps a) Shadow Less and Grayscale Image b) Gray Image Thresholding to Convert the Image to a Binary Image and c) Determined Parts that are Detected by the Nearest Neighbor's Segmentation.



(a)                              (b)

**Figure 6.** Combining the Images, a) Obtained Surface Image of the Rail Head b) The Converted Image Mask for the Video.

Error rates obtained from the performance analysis are evaluated. This assessment is calculated using the root mean square percent error rate. Calculations are performed using equation (7).

$$x_{rms} = \sqrt{\frac{1}{n}\sum_{i-1}^{n} x_i^2}$$ (7)

where n refers to total number of images and $x_{rms}$ represents the total error rate.

Equation (7) is the percentage of squares of errors divided by the number obtained by taking the square root of the value of the total value of the average percentage error values performance.

As a result of the above mentioned algorithms, binary images are obtained. An inference is made using the pixel values of these binary images. The ratio of the number of white pixels to the number of black pixels in the resulting image gives us information about the wear in the rail. In Equation 8, the ratio of the white pixels to the black pixels of the result images is also shown. This rate is calculated as follows.

$$RWB = \frac{NWP}{NBP}$$
(8)

where NWP is the number of white pixels in the resulting image, NBP is the number of black pixels and RWB is the ratio of the number of white pixels to the number of black pixels. An image belonging to a rail known to be healthy was applied to the above mentioned image processing algorithms. The resulting binary image was handled as a result of these algorithms. The number of white pixels in the binary image constituted the NWP parameter. Likewise, the number of black pixels in the binary image constituted the NBP parameter. The ratio of these two values formed a RWB value. In this way the RWB value for a healthy rail was found to be 0.2515. As the amount of wear on the rail increases, the value of the RWB decreases. The difference between the RWB value of a faulty rail and the RWB value of a healthy rail indicates the failure rate of the faulty rail.

Another performance criteria of the study is the detection rate. The detection rate is calculated in equation (9).

$$OTO = \frac{1}{n}.\sum_{i=1}^{n} TO$$
(9)

where OTO is the average amount of the rail surface detection rate, n is total number of images and TO is the rail surface for the images.

$$OHO = \frac{1}{n}.\sum_{i=1}^{n} HO$$
(10)

where OHO is the average error rate, n is total number of images and HO is the error rate for detection of the rail surface.

## 4    EXPERIMENTAL RESULTS

IN this paper, two approaches were proposed. For the Rail Measurement Approach, we created an experimental setup with a laser source and a CCD camera. For the Fault Diagnosis Approach we used a CCD camera. The wear on the surface of rail heads have been asked to be identified. For this process, rail video images are divided into frames with each displayed in such a way to express a 50 cm rail. The aforementioned image processing and image analysis steps were applied on each frame. In practice, it was determined to use the video in different environments and in different light variations to obtain the images. First, the image is made free from noise from the video and the shadow removal is applied so there is no gradation on the rails. This way, the images are ready for processing. The rail images that are ready to process are made of said process for ready for detecting wear and deterioration of the surface. This detection process is done in two different ways. The first is the nearest neighbor classification determined by detecting the edge of the second path rail line head using the Hough transform. This is done by combining the two processed rail images to increase the possibility of finding the correct operation. If the images are showing different positions of the rail surface detected by the Hough and KNN, then the surface should be scanned again.

Figure 7 shows the different rail images obtained as the proposed approach result.

An image belonging to a rail known to be healthy was applied to the above mentioned image processing algorithms. The resulting binary image was handled as a result of these algorithms. The number of white pixels in the binary image constituted the NWP parameter. Likewise, the number of black pixels in the binary image constituted the NBP parameter. The ratio of these two values formed the RWB value. In this way the RWB value for a healthy rail was found to be 0.2515. As the amount of wear on the rail increases, the value of the RWB decreases. The difference between the RWB value of a faulty rail and the RWB value of a healthy rail indicates the failure rate of the faulty rail.

Figure 7 is also free from noise and shadows of the original images and the original image taken from the track that was applied and combined with the results of the KNN and Hough Transform image is shown. Figure 8 from wear on the surface of the algorithm performed by railhead suggests distortion and cracks were detected successfully.

Figure 8 shows the RWB values of the 55 images obtained in this study.

Success rates are found with the percentage of the number of the rail surface detected pictures and the total picture. The results of the wear on the rail head that was used in this study are shown in Table 1.

The results obtained in accordance with the amount of pixels in the image surface of the rail, the rail surface of the detected pixel amount, the probability of detecting and error rates are shown in the graph of Figure 9.

The results of the implementation are evaluated on images with different sizes. The error rates obtained in the study are given in Table 2. These results are obtained from images with different dimensions.
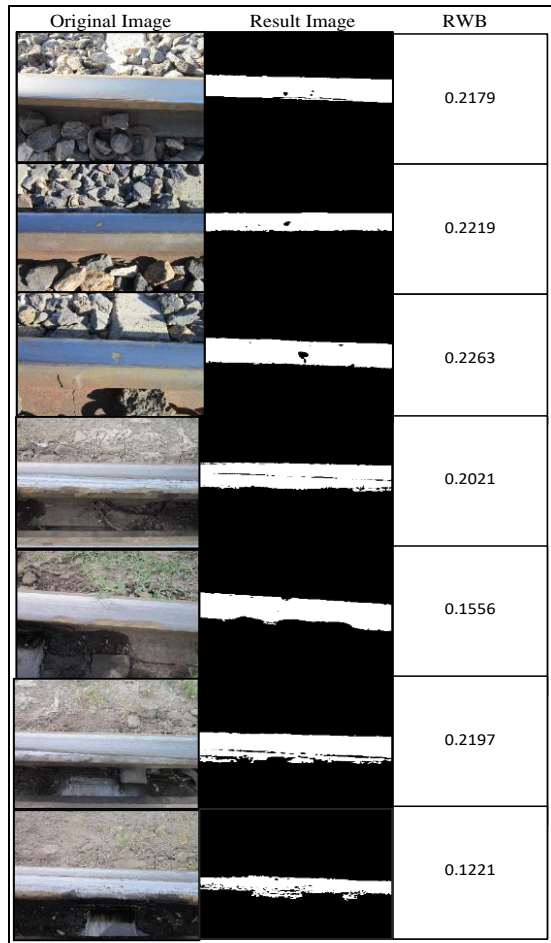
| Original Image | Result Image | RWB |
|---|---|---|
| | | 0.2179 |
| | | 0.2219 |
| | | 0.2263 |
| | | 0.2021 |
| | | 0.1556 |
| | | 0.2197 |
| | | 0.1221 |

**Figure 7.** The Results Obtained from Different Rail Images.



**Figure 8.** RWB Values of the Obtained Images.

**Table 1.** Success Rate

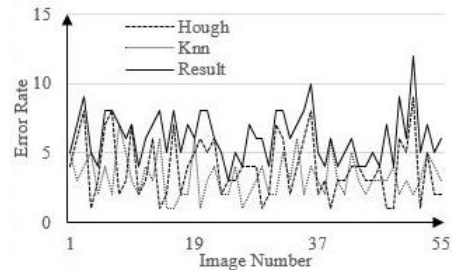| | The Surface of the Rail Head |
|---|---|
| Success rate of the Hough Transform | 75 % |
| Success rate of the KNN | 89 % |
| Success rate of the our algorithm | 96 % |
| Number of Total image | 55 |



**Figure 9.** Performance Results (RM: Amount of Pixels in the Rail Surface, T: Detected, TO: Detection Rate, HO: Error Rate).

**Table 2.** Error Rates for Images with Different Sizes

| No | Size (Pixel) | Positive Error Rate | Negative Error Rate |
|---|---|---|---|
| 1 | 1280 X 720 | 1.12 | 0.92 |
| 2 | 800 X 450 | 1.50 | 2.18 |
| 3 | 640 X 360 | 2.01 | 2.30 |
| 4 | 160 X 90 | 2.20 | 2.43 |

Figure 10 shows the error rates that occur during the detection of the pixels on the rail images. The error rates of the Hough, KNN and the proposed method are shown separately.

The algorithms were performed on a PC with Intel 3.30 GHz CPU and 64 GB of memory, and Windows 10 pro as the operating system. We used MATLAB 2015b software to evaluate the proposed algorithms. The success criteria of the algorithms are based on the RWB values mentioned in the proposed method. The algorithms were applied to the images obtained under real physical conditions.
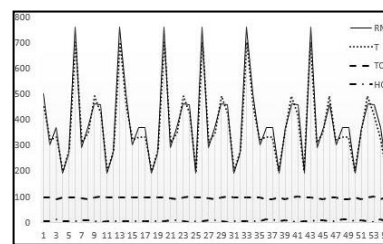


**Figure 10.** Error Rate of the Pixels from the Rail Images.

## 5    CONCLUSION

TWO approaches are proposed in this article. The rail measurement approach and the fault diagnosis approach. In the rail measurement approach, the rail is monitored by a laser source mounted on the train and a CCD camera. Images of the reflected laser lines were taken. Using these images, the rail's points cloud was created. This point cloud gives information related to the measurements of the rail. In the fault diagnosis approach, the rail images are filtered to remove noise. A shadow removal algorithm was applied to remove light variations from the rail images. The Hough Transform and the KNN

segmentation algorithms performed detection for wear of the rail surface. An RWB value was generated from the black and white pixels in the latest image. When the RWB value of the faulty rail is compared to the RWB value of the healthy rail, the fault grade of the rail can be determined.

As the number of high-speed trains and railway vehicles increases, the importance of detecting wear and deterioration on the rail head also increases. In this paper, the wear and cracks on the surface of the rail head are detected by using image processing and analysis techniques. The image that is captured by the camera is prepared for image processing and analysis operations. The image is taken from the railways while the train is on the move, so the image can be distorted. Noise removal filters are applied to provide a clearer image. Shadows may occur with effects of light and objects on the rail, causing different shades on the rails. These shadows pose problems for detection while the rail is analyzed using color segmentation. In this work, light variations are removed so ambient light independent detection is possible. The surface of the rail head is detected by two different methods and two different result images are obtained. By combining these two result images belonging to the same image, the error rate is minimized. The RWB values were obtained from the resulting images. These RWB values were compared with the values of the healthy rail. Therefore, the fault diagnosis has been carried out. In the proposed method, the wear on the surface of the rail head can be detected as contactless. As seen from the experimental results, the wear on the rail head can be detected with high accuracy using this method.

The non-contact rail profile measurement is also mentioned in this paper. Images were taken using a laser source and a camera. The rail was scanned vertically and horizontally by the laser source. In this method, the point cloud of the rail profile was obtained.

## 6    ACKNOWLEDGMENT

## 7    REFERENCES

A. Ekberg, E. Kabo, (2005). Fatigue of railway wheels and rails under rolling contact and thermal loading – an overview. *Wear,* 258, 1288-1300.

A. M. Boronahin, A.S. Kukaev, D.Y. Larionov, L.N. Podgomaya, R. V. Shalymov, E.D. Bokhman (2016). Optical profilometers for rail track diagnostics, *NW Russia Young Researchers in Electrical and Electronic Engineering Conference (ElConRusNW),* DOI:10.1109/ElConRusNW.2016.7448206.

A. M. Boronahin, Y. V. Filatov, D. Y. Larionov, L. N. Podgomaya, R. V. Shalymov (2015). Measurement system for railway track condition monitoring, *Young Researchers in Electrical and Electronic Engineering Conference,* DOI: 10.1109/ ElConRus NW.2015.7102252.

C. Alippi, E. Casagrande, F. Scotti, V. Piuri (2000). Composite real-time image processing for railways track profile measurement. *Instrumentation and Measurement,* 49(3), 559-564.

C. Alippi, E. Casagrande, M. Fumagalli, F. Scotti, V. Piuri, L. Valsecchi (2002). An embedded system methodology for real time analysis of railways tracks profile, *Instrumentation and Measurement Technology Conference,* 1, 747-751.

E. A. Garcia, S. S. Flores, D.A. D. Romeo (2013). Intelligent Fault Diagnosis in Nonlinear Systems, *Intelligent Automation and Soft Computing,* doi.10.1080/10798587.2013.861963, pp. 201-212.

G. D. Finlayson, M. S. Drew, C. Lu (2009). Entropy minimization for shadow removal, *International Journal of Computer Vision,* 85(1), 35-57.

G. Hu, L. Xiong, J. Tang (2015). Heavy rail surface defects detection based on the morphology of multi-scale and dual-structure elements, Chinese Automation Congress (CAC), DOI:10.1109/CAC.2015.7382856.

G. Karaduman, M. Karakose, E.Akin, (2012). Experimental Fuzzy Diagnosis Algorithm Based on Image Processing for Rail Profile Measurement. Mechatronika 2012, Prag.

G. Zumpano, M. Meo (2006). A new damage detection technique based on wave propagation for rails. International Journal of Solids and Structures, 43, 1023-1046.

I. Aydin, M. Karakose, E. Akin (2015). Anomaly detection using a modified kernel-based tracking in the pantograph-catenary system, Expert Systems with Applications, vol.42, 938-948.

J. Chen, C. Roberts, P. Weston, (2008). Fault detection and diagnosis for railway track circuits using neuro fuzzy systems. Control Engineering Practice, 16, 585-596.

K. D. Van, M. Maitournam, H., Moumni, Z., F. Roger (2009). A comprehensive approach for modeling fatigue and fracture of rails. Engineering Fracture Mechanics, 76(17), 2626-2636.

K., T. F. Ma, Y. Vicente, D. Samaras, M. Petrucci, D. L. Magnus (2016). Texture classification for rail surface condition evaluation, Applications of Computer Vision (WACV), DOI:10.1109/WACV.2016.7477597.

L. Jie, L. Siwei, L. Qingyong, Z. Hanqing, R. Shengwei (2009). Real-time rail head surface defect detection: A geometrical approach. IEEE International Symposium on Industrial Electronics, 769-774, 2009. L. Oukhellou, A. Debiolles, T. Denoux, P. Aknin (2010). Fault

diagnosis in railway track circuits using Dempster-Shafer classifier fusion. Engineering Applications of Artificial Intelligence, 23, 117-128.

M. Madia, S. Beretta, U. Zerbst (2008). An investigation on the influence of rotary bending and press fitting on stress intensity factors and fatigue crack growth in railway axles, *Engineering Fracture Mechanics*, 75, 1906-1920.

M. S. Chafi, M. Akbarzadeh-t, M. Moavenian, (2010). A Novel Soft Computing Approach to Component, Fault, Detection and Isolation of CNC X-Axis Drive System"*, Intelligent Automation and Soft Computing*, Vol.16, No.2, pp.177-191.

P. Manso, D. F. Garcia, R. Usamentiaga (2016). Rail flatness measurement method based on virtual rules. *Industry Applications Society Annual Meeting,* DOI:10.1109/IAS.2016.7731913.

Q. Li (2012). A real-time visual inspection system for discrete surface defects of rail heads. *IEEE Transactions on Instrumentation and Measurement.*

R. B. Faiz, S. Singh (2009). Rail profile condition monitoring information analysis of UK rail track, *ICC'09 International Conference on Computing, Engineering and Information*, 191-199.

S. F. Roohi, S. Hajizadeh, A. Nuriez, R. Babuska, B. D. Schutter (2016). Deep convolutional neural networks for detection rail surface defects, *Neural Networks (IJCNN), DOI*: 10.1109/IJCNN.2016.7727522.

S. Judek, L. Jarzebowicz (2016). Analysis of Measurement Errors in Rail Vehicles' Pantograph Inspection System, *Elektronika ir Elektrotechnika,* vol. 22, no. 3.

S. Kaewunruen, A. M. Remennikov (2007). Field trials for dynamic characteristics of railway track and its components using impact excitation technique. *NDT&E International*, 40, 510-519.

U. Zerbst, R. Lunden, K. O. Edel, R. A. Smith (2009). Introduction to the damage tolerance behaviour of railway rails-a review. *Engineering Fracture Mechanics.*

V. B. Valsan, C. Y. Patil, J. M. Patekari (2015). Non-contact rail track parameter measurement, Industrial Instrumentation and Control (ICIC), DOI:10.1109/IIC.2015.7150924.

V. R. Vijaykumar, S. Sangamithirai (2015). Rail defect detection using Gabor filters with texture analysis, DOI:10.1109/ICSCN.2015.7219838.

W. Jin, X. Zhan, B. Jiang (2007). Non-contact rail wear inspecting system based on image understanding. *Mechatronics and Automation*, 5-8 Ağustos, 3854-3858.

Z. Zhiping, L. Fei, Z. Yong (2010). Wavelet analysis of track profile irregularity for Beijing-Tianjin intercity high speed railway on bridge. *International Conference on Intelligent Computation Technology and Automation (ICICTA),* 3, 1155-1158.

## 8    NOTES ON CONTRIBUTORS

**Gulsah Karaduman** received B.S. degree in 2009, M. S. degree in 2013, in Computer Engineering from Firat University, Elazig, Turkey and now she is a Ph. D. student in Computer Engineering from Firat University, Elazig, Turkey. She worked at the Turkish Air Force as a Computer Engineer in 2009-2011. She has been a Research Assistant at Computer Engineering Department, Firat University since 2011. Her research interests include fault diagnosis, computer vision, railway inspection systems.
Email: gkaraduman@firat.edu.tr

**Mehmet Karakose** received B. S. degree in Electrical Engineering from Firat University, Elazig, Turkey, in 1998, M. S. degree in Computer Engineering from Firat University, Elazig, Turkey, in 2001, respectively, and Ph. D. degree in Electrical Engineering (Computer Engineering) from Firat University, Elazig, Turkey, in 2005. He is currently an Associate Professor, and Doctor in the Department of Computer Engineering, Firat University, Turkey. He was a Research Assistant at Computer Engineering Department, Firat University from 1999 to 2005. His research interests include fuzzy systems, intelligent systems, simulation and modeling, fault diagnosis, computer vision, railway inspection systems, and photovoltaic systems.
Email: mkarakose@firat.edu.tr

**Ilhan Aydin** received B.Sc. and M.Sc. degrees in Computer Engineering and Ph.D. degree in Electrical and Electronics Engineering from Firat University, Elazig, Turkey, in 2001, 2006, and 2011, respectively. He is currently an Associate Professor of Computer Engineering at Firat University. His research interests include soft computing, optimization, real-time systems, field-programmable gate array, fault diagnosis and condition monitoring, signal and image processing.
Email: iaydin@firat.edu.tr

**Erhan Akin** was born in Erzincan, Turkey, in 1963. He received B.S. and M.S. degrees in Electrical Engineering and Ph.D. degree in the area of AC Drives from Firat University, Elazig, Turkey, in 1984, 1987, and 1994, respectively. He was with the Department of Electrical Engineering, Firat University, first as an Assistant Professor and then as an Associate Professor of Electrical Machines. He is currently a Full Professor of Computer Engineering at Firat University. His main research interests are in power electronics, digital control of variable-speed ac drives, fuzzy control and soft-computing techniques. Email: eakin@firat.edu.tr